ADVANCED MATERIALS
www.advmat.de

Revealing the Anion–Solvent Interaction for Ultralow Temperature Lithium Metal Batteries

Jijian Xu, Volodymyr Koverga, An Phan, Ai min Li, Nan Zhang, Minsung Baek, Chamithri Jayawardana, Brett L. Lucht, Anh T. Ngo,* and Chunsheng Wang**

Anion solvation in electrolytes can largely change the electrochemical performance of the electrolytes, yet has been rarely investigated. Herein, three anions of bis(trifluoromethanesulfonyl)imide (TFSI), bis(fluorosulfonyl)imide (FSI), and derived asymmetric (fluorosulfonyl)(trifluoro-methanesulfonyl)imide (FTFSI) are systematically examined in a weakly Li^+ cation solvating solvent of bis(3-fluoropropyl)ether (BFPE). In-situ liquid secondary ion mass spectrometry demonstrates that $FTFSI^-$ and FSI^- anions are associated with BFPE solvent, while weak $TFSI^-$/BFPE cluster signals are detected. Molecular modeling further reveals that the anion–solvent interaction is accompanied by the formation of H-bonding-like interactions. Anion solvation enhances the Li^+ cation transfer number and reduces the organic component in solid electrolyte interphase, which enhances the Li plating/stripping Coulombic efficiency at a low temperature of −30 °C from 42.4% in TFSI-based electrolytes to 98.7% in 1.5 M LiFTFSI and 97.9% in LiFSI-BFPE electrolytes. The anion–solvent interactions, especially asymmetric anion solvation also accelerate the Li^+ desolvation kinetics. The 1.5 M LiFTFSI-BFPE electrolyte with strong anion–solvent interaction enables $LiNi_{0.8}Mn_{0.1}Co_{0.1}O_2$ (NMC811)||Li (20 µm) full cell with stable cyclability even under −40 °C, retaining over 92% of initial capacity (115 mAh g^{-1}, after 100 cycles). The anion–solvent interactions insights allow to rational design the electrolyte for lithium metal batteries and beyond to achieve high performance.

1. Introduction

The global energy transition is set to push batteries into broader applications and operation in harsher conditions.[1] The temperature-abuse tolerance of lithium metal batteries is urgently needed for electric vehicles or large-scale energy storage technologies, especially under the extreme condition of low temperatures.[2] Commercial carbonate-based electrolytes are incapable of low-temperature operation below −20 °C, confronting freezing issues and resultant sluggish ion transportation through the interphasial layers.[3] Electrolyte is the key to achieving reversible lithium plating/stripping at ultra-low temperatures (e.g., below −20 °C).[4]

The rational electrolyte design mainly focuses on tuning the Li^+ solvation structure since the solvation structure not only affects Li^+ transport in the bulk electrolyte but also changes the solid–electrolyte interphase (SEI) composition.[5] Li^+ solvation structure has been extensively investigated experimentally and theoretically.[6] Recently, anion-participated solvation structure was also reported, which can also change the SEI formation and Li^+ desolvation kinetics.[7] However, the anion–solvent interactions are still not fully understood even in the simplest single-salt, single-solvent electrolyte system. The anion–solvent interaction can have several benefits. First, anion–solvent interaction facilitates lithium salt dissociation, leading to higher ionic conductivity. Second, stronger anion–solvent interaction limits anionic mobility and enhances the Li^+ transference number (t_+). Finally, anion–solvent interaction

J. Xu, A. Phan, A. min Li, N. Zhang, M. Baek, C. Wang
Department of Chemical and Biomolecular Engineering
University of Maryland
College Park, MD 20742, USA
E-mail: jijianxu@cityu.edu.hk; cswang@umd.edu

J. Xu
Department of Chemistry
City University of Hong Kong
Kowloon 999077, Hong Kong

V. Koverga, A. T. Ngo
Department of Chemical Engineering
University of Illinois Chicago
Chicago, IL 60608, USA
E-mail: anhngo@uic.edu

V. Koverga, A. T. Ngo
Materials Science Division
Argonne National Laboratory
Lemont, IL 60439, USA

C. Jayawardana, B. L. Lucht
Department of Chemistry
University of Rhode Island
Kingston, Rhode Island 02881, USA

The ORCID identification number(s) for the author(s) of this article can be found under https://doi.org/10.1002/adma.202306462

DOI: 10.1002/adma.202306462

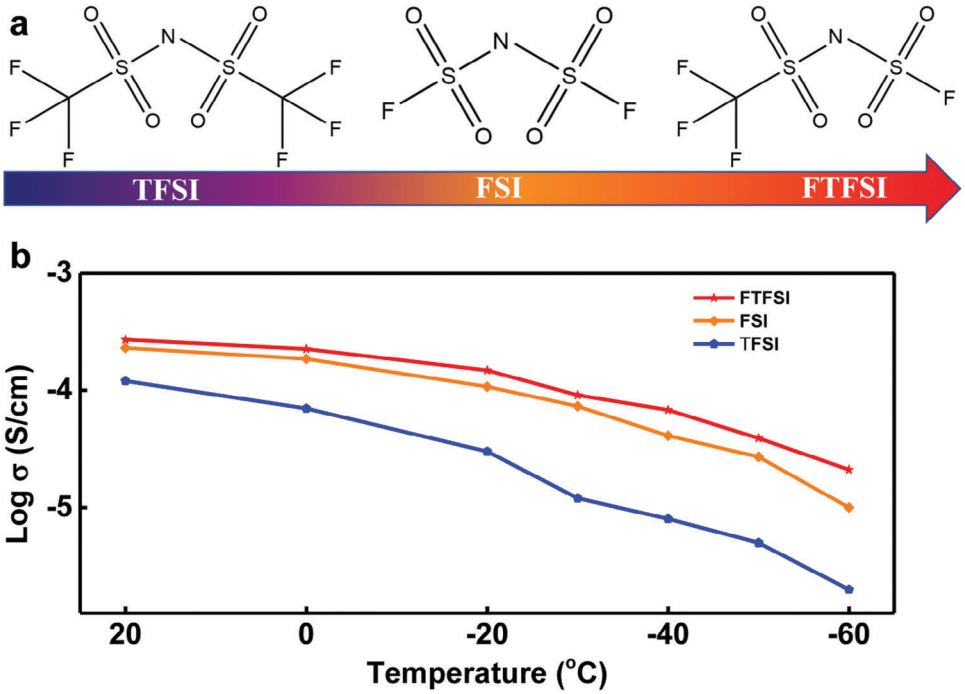

Figure 1. Properties of the electrolytes. a) Chemical structures of the TFSI, FSI, FTFSI anions. b) Temperature dependence of the conductivity of LiTFSI, LiFSI, LiFTFSI-BFPE electrolytes.

suppresses solvent-reduction and promotes the formation of anion-derived inorganic-rich SEI, which enhances the Li plating/stripping Coulombic efficiency (CE).

This work aims to gain insights into the anion–solvent interactions and their effect on low-temperature performance. A group of electrolytes containing various lithium salts (LiFTFSI, LiFSI, LiTFSI) and partially fluorinated ether solvent, BFPE, were systematically investigated. BFPE, with weakly interacting with Li^+, makes the anion solvent more visible. Using both experimental characterizations and theoretical calculations, we identify that the distinct anion–solvent interaction in 1.5 M LiFTFSI-BFPE electrolyte enhanced ionic conductivity and improved lithium metal performance at a low temperature of <−30 °C. 1.5 M LiFTFSI-BFPE electrolyte enables Li plating/stripping CE at −30 °C to reach a record-high value of 98.7%, and 2.0 mAh cm^{-2} NMC811||Li (2× excess) full cells to charge/discharge at an ultra-low temperature of −40 °C and deliver a high reversible capacity of 115 mAh g^{-1} with negligible capacity decay over 100 cycles.

2. Results and Discussion

2.1. Physicochemical Properties and Solvation Structure

To investigate the anion–solvent interaction, three representative anions of bis(trifluoromethanesulfonyl)imide (TFSI), bis(fluorosulfonyl)imide (FSI), and asymmetric (fluorosulfonyl)(trifluoro-methanesulfonyl)imide (FTFSI) with similar dissociation energies for Li^+-$FTFSI^-$, Li^+-$TFSI^-$, and Li^+-FSI^- were systematically examined.[8] The anion solvation of other asymmetric anions remains to be explored. As shown in **Figure 1**a, the FTFSI anion is an asymmetrical hybrid between the TFSI and FSI anions. LiFTFSI-BFPE electrolyte has a higher Li-ion conductivity than that of LiFSI or LiTFSI-BFPE electrolytes over the whole temperature range between −60 and +20 °C due to its asymmetry (Figure 1b). At 20 °C the electrolytes containing LiFTFSI and LiFSI possess comparable ionic conductivity, which is consistent with the results reported in the literature.[9] When the temperature drops, for example, to -60°C, LiFTFSI-containing electrolyte has a higher ionic conductivity of 0.021 mS/cm compared to 0.010 mS/cm for LiFSI-BFPE electrolyte, not to mention the LiTFSI-BFPE electrolyte. Specific conductivity values are listed in Table S1. The enhanced conductivity could originate from the anion–solvent interaction which facilitates the salt dissociation. The thermal behavior of electrolytes with LiTFSI, LiFSI, and LiFTFSI in BFPE solvent was investigated by using scanning calorimetry (DSC), which indicated no crystallization or melting (Figure S1, Supporting Information). Note that LiFTFSI possesses the lowest melting point among various lithium salts, as summarized in Table S2 (Supporting Information), despite that the dissociation energies are found to be similar for Li^+-$FTFSI^-$, Li^+-$TFSI^-$, and Li^+-FSI^-.

The strong interaction between FTFSI anion and BFPE solvent was identified using ^{19}F NMR signals of different electrolytes, which show an upfield shift in the sequence of TFSI-BFPE < FSI-BFPE < FTFSI-BFPE (**Figure 2**a). The role of anions was further investigated using attenuated total reflection-Fourier transform infrared (ATR-FTIR) spectroscopy. As presented in Figure 2b, the characteristic peaks of the C—O—C bond in free BFPE are located at 1120, 1052, 1008, and 949 cm^{-1} (Ash line). Meanwhile, double peaks observed in the region of 1300–1400 cm^{-1} are designated as $-SO_2$ stretching of lithium salts.[10] Interestingly, new peaks around 830 cm^{-1} arise for FTFSI-BFPE

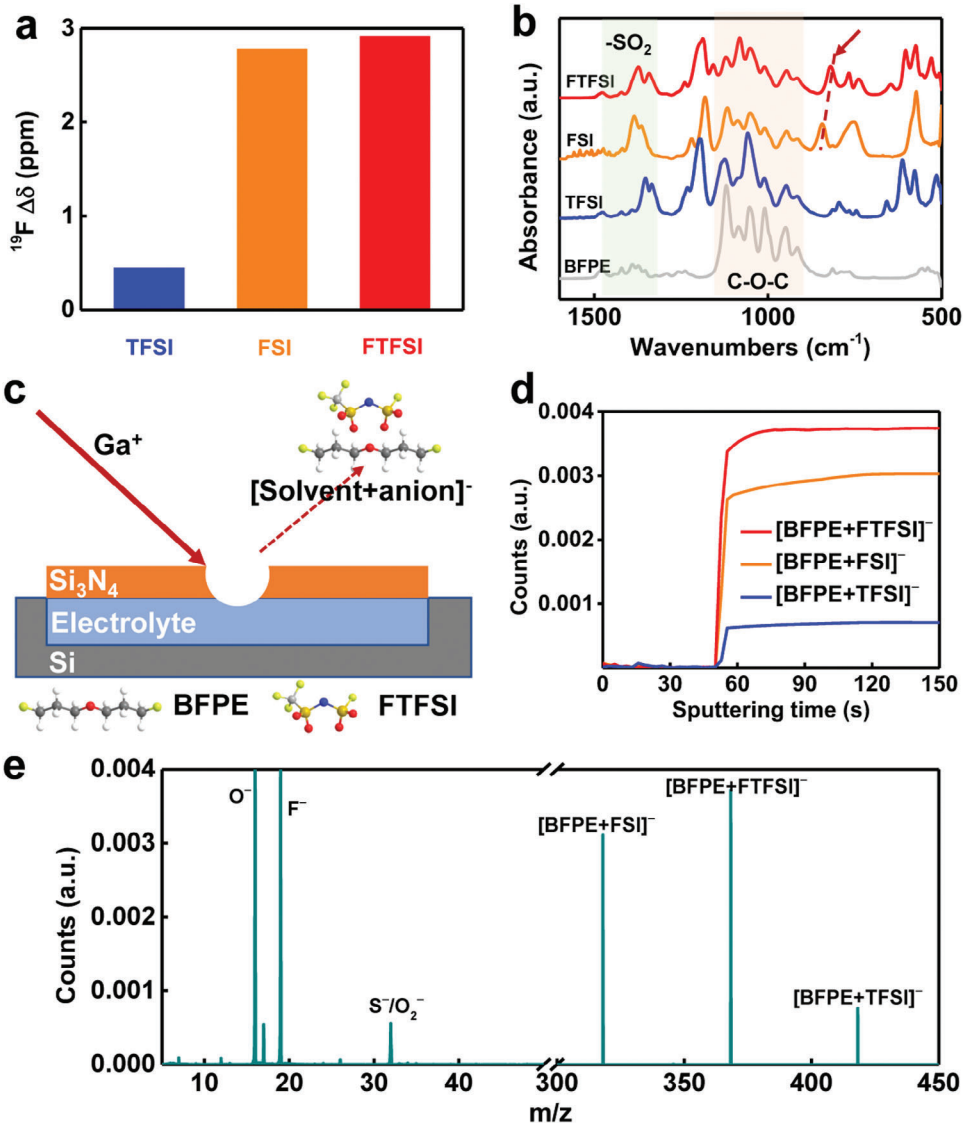

Figure 2. Anion–solvent interactions. | a) summary of $\Delta\delta$ (^{19}F NMR spectra of BFPE solvent) in LiTFSI, LiFSI, LiFTFSI-BFPE electrolytes. b) ATR-FTIR spectra of the electrolytes and bare BFPE solvent. Green zone: -SO_2 vibration, orange zone: C-O-C stretch. c) Schematic setup of an in-situ liquid SIMS cell assembled by silicon support grids with silicon nitride membranes. A ~1 µm diameter hole was then pouched by a focused ion beam during the in-situ SIMS analysis. d) Depth profiles and e) mass spectra of 0.5 M LiFSI+0.5 M LiFTFSI+0.5 M LiTFSI in BFPE electrolytes in the negative ion mode. For about 50 s, the Si_3N_4 film is penetrated and exposes the electrolyte within the cell.

and FSI-BFPE electrolytes that were outlined by the red dashed line and the arrow, indicating the anion–solvent interaction. The anion–solvent interaction limit anionic mobility and enhances the Li^+ transference number (t_+). As a result, high t_+ (0.86 for FTFSI-BFPE, and 0.83 for FSI-BFPE) are obtained as presented in Figure S2 (Supporting Information).

The anion–solvent interactions were also investigated by using in-situ liquid secondary ion mass spectrometry (SIMS). All three anions of FTFSI, FSI, and TFSI were dissolved at the same concentration of 0.5 M in BFPE solvent. As illustrated in Figure 2c, operand analysis of liquid electrolytes is feasible by drilling a small hole so that a probing primary beam can interact with the electrolyte.[11] The depth profiles of representative [solvent-anion] clusters are shown in Figure 2d. [BFPE-FTFSI]$^-$, [BFPE-FSI]$^-$, and [BFPE-TFSI]$^-$ signals were detected immediately following the Si_3N_4 film was sputtered through (≈50 s), suggesting that anions form an association with BFPE solvent. The intensity of the peaks increases from [BFPE-TFSI]$^-$ to [BFPE-FSI]$^-$ to [BFPE-FTFSI]$^-$, indicating the interaction between the anion and BFPE solvent becomes stronger and stronger. At 100 s, when the signals became relatively stable, mass spectra were retracted, as presented in Figure 2e. O^- and F^- peaks dominate the spectra, which may come from the damaged lithium salts and BFPE solvent. More importantly, the solvated anion peaks, namely, [BFPE-TFSI]$^-$ (m/z = 418), [BFPE-FSI]$^-$ (m/z = 318), and [BFPE-FTFSI]$^-$ (m/z = 468) were clearly observed. The intensity of [BFPE-FTFSI]$^-$ is higher than [BFPE-FSI]$^-$ and both are almost one order of magnitude higher

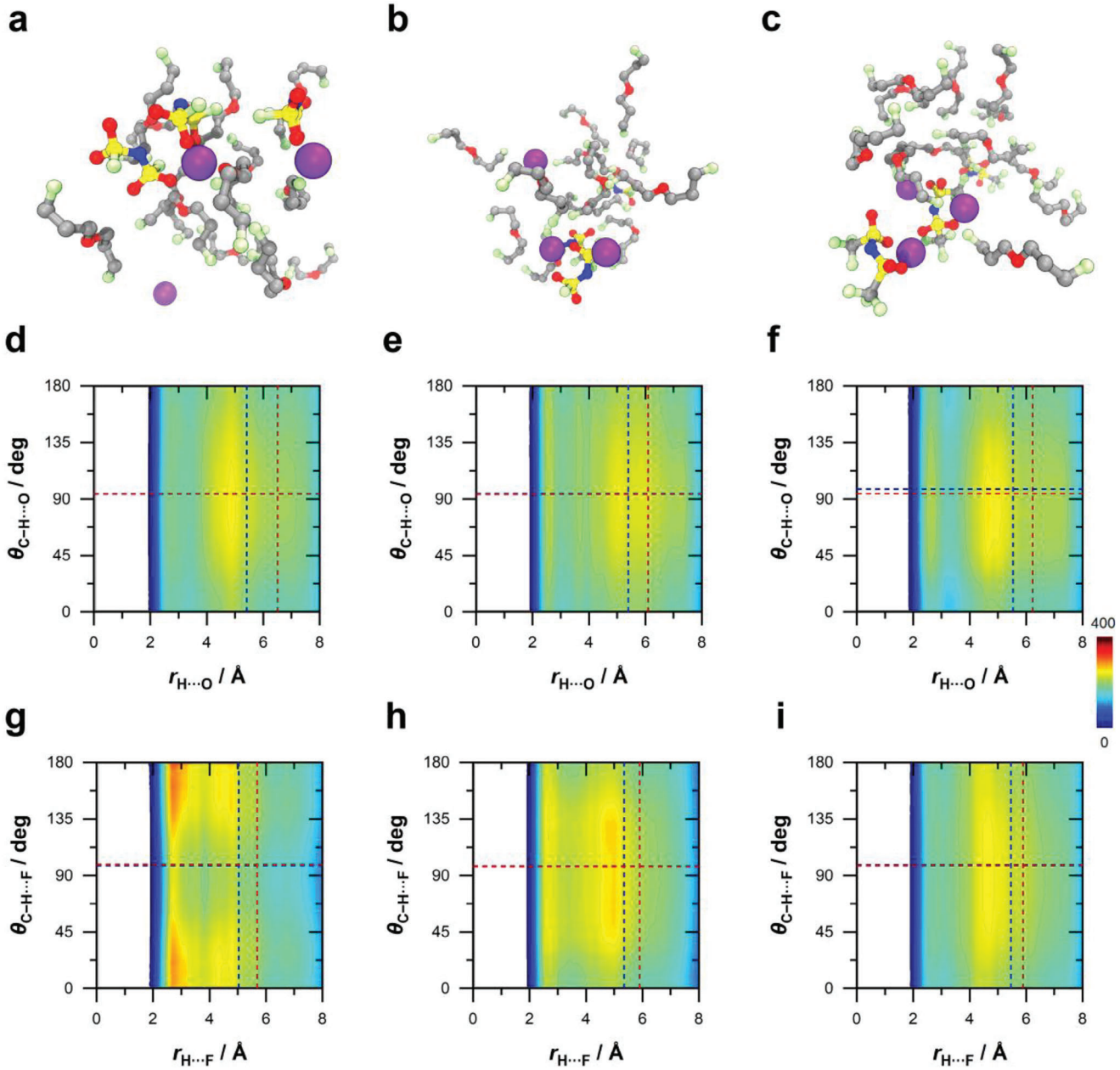

Figure 3. Anion–solvent interactions via simulations. | a–c) Snapshots of the 1.5 M LiFSI- (a), LiFTFSI- (b), and LiTFSI-based (c) BFPE electrolytes equilibrated by means of AIMD simulation at 298 K. Color codding of the elements: gray — C, red — O, lime — F, yellow — S, blue — N and violet — Li atoms (H atoms are hidden for clarity). d–i) Ion-molecular interactions between solvent molecules, comprising H-bonding distances based on H•••O (d–f) and H•••F (g–i) atom pairs of BFPE and FSI^- (d,g), $FTFSI^-$ (e,h) and $TFSI^-$ (f,i) and corresponding H-bonding angles, C–H•••F and C–H•••O, represented in terms of combined radial/angular distribution function for the first nearest neighboring site, in 1.5 M LiFSI/FTFSI/TFSI-based BFPE system analyzed employing AIMD simulation at 298 K. For dashed vertical and horizontal lines stands for the average H-bonding distance and angle, respectively, analyzed at 298 (red) and 233 K (blue) using classical MD simulation.

than that of $[BFPE\text{-}TFSI]^-$, confirming stronger BFPE-FTFSI interaction.

Molecular modeling, particularly ab initio (AIMD) and classical molecular dynamics (MD), was employed to understand anion–solvent interaction at the ion-molecular level. Representative snapshots of LiFSI-BFPE (**Figure 3**a), LiFTFSI-BFPE (Figure 3b), and LiTFSI-BFPE (Figure 3c) indicate that BFPE solvent mainly coordinated by the F atom concerning the Li^+ cation. Detailed Li coordination statistics suggest the Li coordination ability in the order of $TFSI^- > FTFSI^- > FSI^-$ (Figure S3, Supporting Information). In addition to Li^+ cation solvation, anion solvation is also observed. An in-depth analysis of AIMD simulations confirms that the FSI^- and $FTFSI^-$ anions have high interaction with the solvent. As shown in Figure 3g–i, the strength of anion–solvent interactions is accompanied by the formation of H-bonding-like interactions between H and

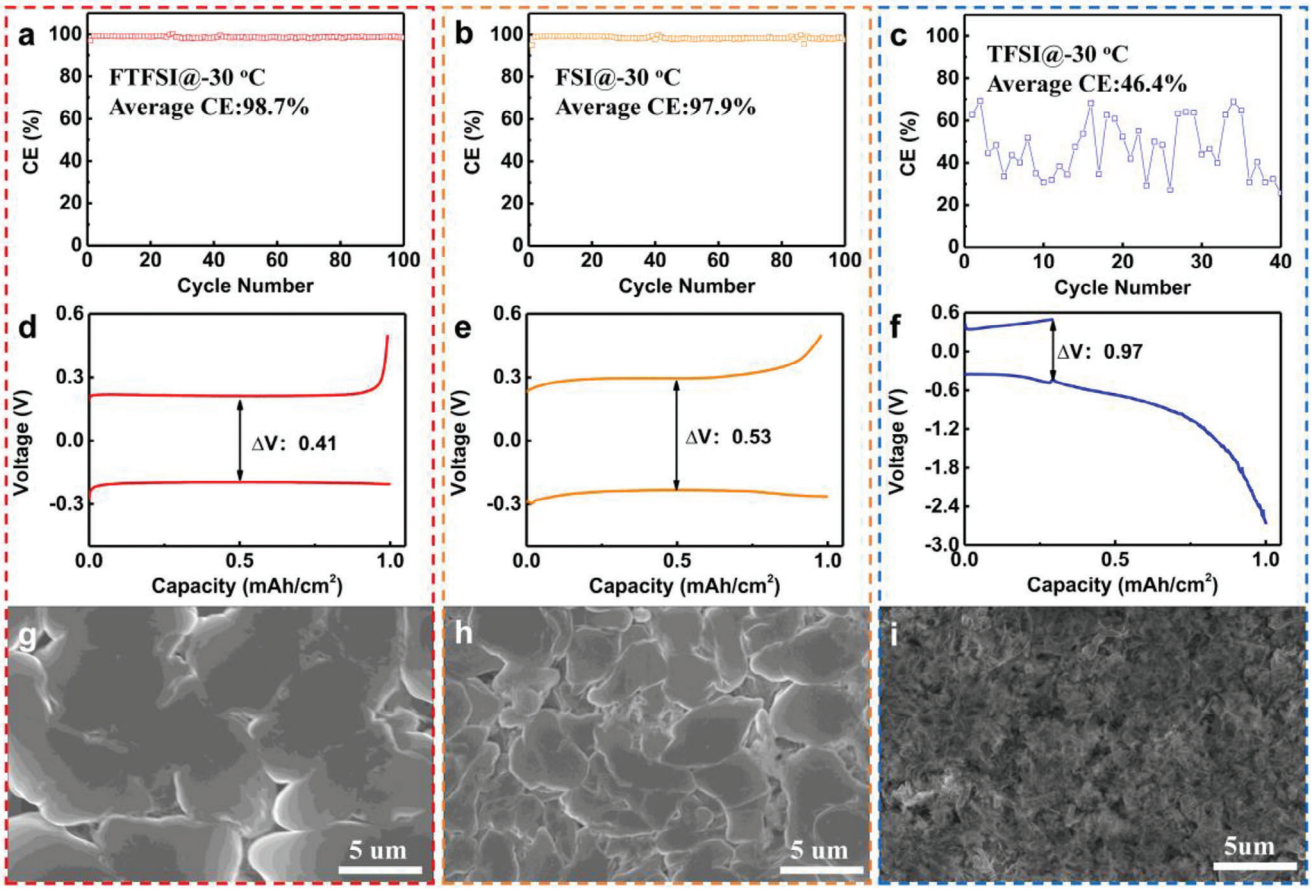

Figure 4. Li metal plating/stripping efficiency at an ultralow temperature of −30 °C. | a–c) Coulombic efficiency (CE) versus cycle number, and d–f) selected voltage profiles of the 10th cycle for Li||Cu cells at a current density of 0.25 mA cm^{-2} using LiFTFSI, LiFSI, and LiTFSI-BFPE electrolytes, respectively. g–i) Corresponding SEM images of deposited Li on copper foil in different electrolytes.

F. More interestingly, it is found that the temperature effect is strongly pronounced for both H•••F and H•••O interactions between solvent and anion (Figure 3d–i).

The anion–solvent interaction has been directly confirmed by in situ SIMS. However, it is still relatively weak compared to the Li^+-solvent interaction at room temperature as suggested by simulation. A typical anion solvation energy in the 20–30 kcal mol^{-1} range is less than the corresponding Li^+ solvation energy of ≈32 kcal mol^{-1}.[12] The impact of anion–solvent interaction on the electrochemical performance of Li metal anodes is small at room temperature. As shown in Figure S4 (Supporting Information), the cycling performance of Li plating/stripping in LiFTFSI-BFPE electrolytes is slightly better than or similar to that in LiFSI-BFPE electrolytes, but Li CE and overpotential in both electrolytes are much better than that in LiTFSI-BFPE. Since the reversible stripping and plating of Li metal anode under low temperatures is extremely challenging due to the sluggish ion transport, the benefit of anion–solvent interaction is largely enhanced. The cycling performance of Li metal plating/stripping on a Cu electrode at a current density of 0.25 mA cm^{-2} under −30 °C is shown in **Figure 4**a–c. The CE of the LiFTFSI-BFPE electrolyte is 96.8% for the first cycle (Figure 4a), which quickly rises to above 99% within three cycles, showing superior cycling performance with a high average CE of 98.7% over 100 cycles. The LiFSI–BFPE electrolyte is slightly worse than the LiFTFSI-BFPE electrolyte, showing a slightly lower average CE of 97.9% (Figure 4b). In sharp contrast, the average CE of the LiTFSI-BFPE electrolyte dramatically drops to 46.4%, presenting poor cycling performance (<40 cycles, Figure 4c). Moreover, the CEs with LiFTFSI-BFPE electrolyte were tested to be 99.3%, 99.2%, 99.1%, and 98.8% at 25, 0, −20, and −30 °C based on a modified CE measurements protocol (Figure S5, Supporting Information).[13]

In addition, Li||Cu cell with LiFTFSI-BFPE electrolyte possesses the lowest overpotential, 410 mV (LiFTFSI-BFPE, Figure 4d) < 530 mV (LiFSI-BFPE, Figure 4e) << 970 mV (LiTFSI-BFPE, Figure 4f). The fast reaction kinetics of Li plating/stripping in LiFTFSI-BFPE electrolyte is attributed to the high ionic conductivity and LiF-rich SEI in LiFTFSI-BFPE electrolyte.

To reveal the role of anion–solvent interaction in dictating the electrochemical properties of Li metal batteries, scanning electron microscopy (SEM) and X-ray photoelectron spectroscopy (XPS) of cycled electrodes were performed. Figure 4g–i shows the morphology of deposited lithium metal on copper foil under −30 °C for LiFTFSI, LiFSI, and LiTFSI-BFPE electrolytes, respectively. For LiFTFSI-BFPE and LiFSI-BFPE electrolytes,

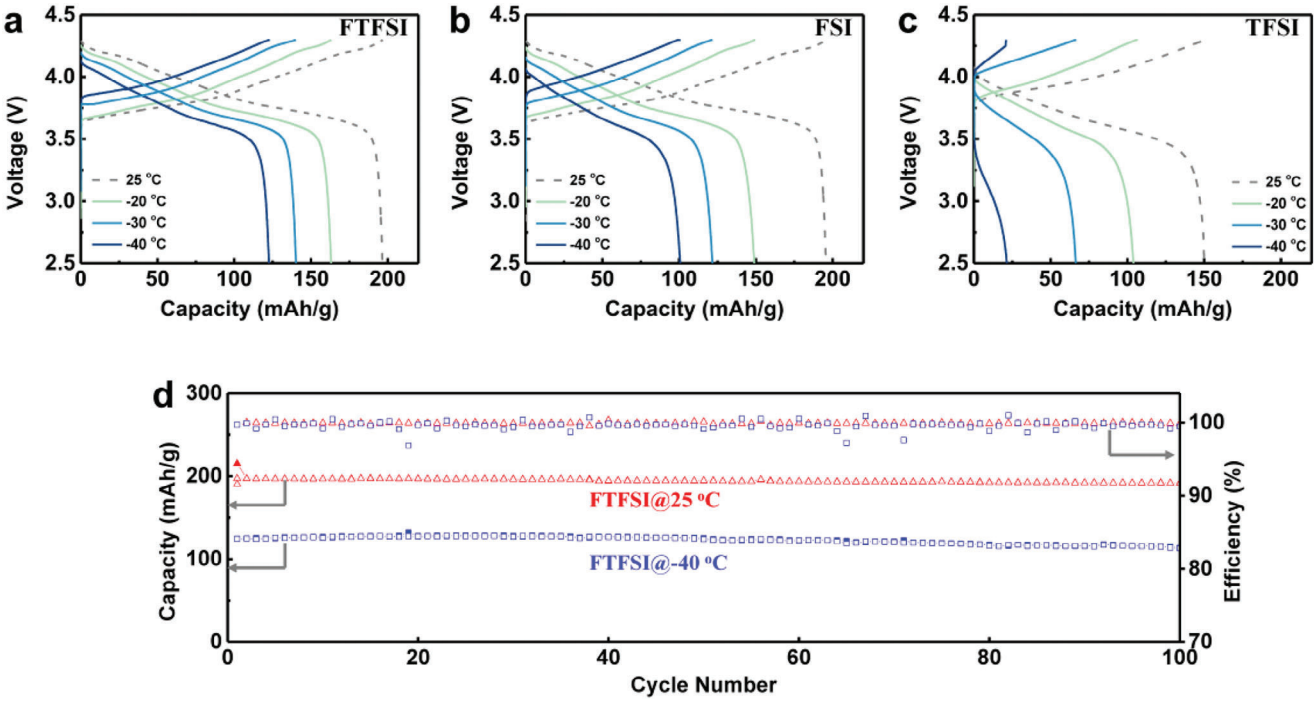

Figure 5. | Electrochemical performance of full cells. Typical voltage profiles of NMC811 (2.0 mAh cm^{-2})||Li (20 µm, 2× excess) full cells in the electrolytes of a) LiFTFSI-BFPE, b) LiFSI-BFPE, and c) LiTFSI-BFPE at 0.1 C for charging/discharging under various temperatures. d) Long cycling performance of NMC811||Li cells in the electrolyte of LiFTFSI_BFPE at 25 and −40 °C.

the surface of deposited lithium is flat. The Li particle size in LiFTFSI-BFPE is ≈10 µm (Figure 4g) and ≈5 µm in LiFSI-BFPE electrolytes (Figure 4h). In contrast, a large amount of needle-like and porous dendritic Li is observed for deposited Li in the LiTFSI-BFPE electrolyte (Figure 4i). The SEM images evidence that LiFTFSI-BFPE and LiFSI-BFPE electrolytes are beneficial for forming more dense and compact Li deposits, corresponding to higher CE for Li plating/stripping.

XPS analysis of Li deposits on copper was further conducted to investigate the nature of the SEI layers. Figure S6 (Supporting Information) summarizes the compositions of the SEI layer formed in the three electrolytes together with detailed C *1s*, O *1s*, and F *1s* spectra as a function of different etching times. According to the results, both the SEI formed in LiFTFSI-BFPE and LiFSI-BFPE electrolytes are inorganic-rich, with LiF and Li_2CO_3 being the predominant species, while the SEI formed in LiTFSI-BFPE electrolyte contains more organic contents. As reported, the SEI layer formed in LiTFSI-based electrolytes is mainly dominated by solvent reduction, resulting in more organic species.[9,14] Moreover, the C-F bond in TFSI anion is less vulnerable to reduction than the S-F bond in FSI and FTFSI anions,[15] which explains why only a small amount of LiF could be detected on the SEI layer deriving from LiTFSI–BFPE electrolyte. Simulation results verify the FTFSI anion promotes a higher rate of decomposition: $FTFSI^- > TFSI^- > FSI^-$, leading to the formation of inorganic products like Li_2O and LiF in the existence of BFPE solvent (Figure S7, Supporting Information).

The anodic stabilities of the LiFTFSI, LiFSI, and LiTFSI-BFPE electrolytes are displayed in Figure S8a (Supporting Information), showing low anodic currents of <0.005 mA cm^{-2} at 4.5 V versus Li/Li^+ for all three electrolytes. The more stringent floating tests confirmed the high stability of the LiFTFSI-BFPE electrolytes at high voltages (Figure S8b, Supporting Information), suggesting the capability to support high-voltage cathodes such as $LiNi_{0.8}Mn_{0.1}Co_{0.1}O_2$ (NMC811).[16] Accordingly, NMC811 (2.0 mAh cm^{-2})||Li (20 µm, 2× excess) full cells were assembled to illustrate the anion–solvent effect under various temperatures. As shown in **Figure 5**a, the cells using LiFTFSI-BFPE electrolyte deliver 196, 163, 140, and 123 mAh g^{-1} (based on the cathode), when both charged and discharged at 25, −20, −30, and −40 °C. Slightly lower capacity retention in the LiFSI-BFPE electrolyte is displayed in Figure 5b, with outputting capacities of 196, 149, 121, and 101 mAh g^{-1} at 25, −20, −30, and −40 °C, respectively. In the case of LiTFSI-BFPE electrolyte, a significant ohmic polarization was observed with dramatically reduced capacities (Figure 5c), which is consistent with the ionic conductivity results and uneven lithium deposition. The relative increase in low-temperature capacity retention between LiFTFSI-BFPE and LiFSI-BFPE electrolytes is possibly due to the increased anion–solvent interaction.

As shown in Figure 5d, the LiFTFSI-BFPE electrolyte can fully support stable charging/discharging of the NMC811||Li cells in the voltage range of 2.5–4.3 V at 25 °C. Even when subject to an ultra-low temperature of −40 °C, it retains over 92% of its initial capacity over 100 cycles (Figure 5d). More impressively, NMC811||Li cells were able to charge/discharge at an even lower temperature of −50 and −60 °C. As shown in Figure S9 (Supporting Information), 97.6 mAh g^{-1}, and 39.7 mAh g^{-1} charge capacity can be delivered with LiFTFSI–BFPE electrolyte at −50 and −60 °C, respectively. These full-cell results are consistent with

the Li||Cu efficiencies and in situ SIMS results, indicating that electrolytes with strong anion–solvent interaction are suitable for low-temperature lithium metal batteries.

3. Conclusion

In summary, electrolytes composed of varying lithium salts (LiFTFSI, LiFSI, LiTFSI) dissolved in a fluorinated BFPE solvent were systematically studied to probe the effect of anion–solvent interaction. Through in-situ SIMS, $[BFPE\text{-}TFSI]^-$ to $[BFPE\text{-}FSI]^-$ species were directly observed, verifying the interaction between anion and solvent. Such anion solvation arises from the formation of both H•••F and H•••O interactions between solvent and anion, as indicated by molecular modeling. It was found that only electrolytes with relatively stronger anion–solvent interaction could provide reversible lithium plating/stripping with an average CE close to 99% at −30 °C. Moreover, 2.0 mAh cm^{-2} NMC811|| Li full cells with 2× excess lithium employing 1.5 M LiFTFSI-BFPE electrolyte with strong anion–solvent interaction achieved 100 cycles at an ultra-low temperature of −40 °C with minimal capacity decay while maintaining 63% of their room temperature capacity. This work demonstrates that anion–solvent interaction may be another unexplored area of rational electrolyte design for lithium metal batteries and beyond.

Supporting Information

Supporting Information is available from the Wiley Online Library or from the author.

Acknowledgements

This work is supported by the Assistant Secretary for Energy Efficiency and Renewable Energy, Office of Vehicle Technologies of the US Department of Energy through the Advanced Battery Materials Research (BMR) Program (Battery500 Consortium Phase 2) under DOE contract No. DE-AC05-76RL01830 from the Pacific Northwest National Laboratory. This work was financially supported by the U.S. Department of Energy ARPA-E grant DEAR0000389. Research was sponsored by the Army Research Laboratory and was accomplished under cooperative agreement number W911NF-20-2-0284.

Conflict of Interest

The authors declare no conflict of interest.

Author Contributions

J.X. conceived the original idea, conducted the experiments, and drafted the manuscript. C.W. directed the project. A.P., A.-M.L., N.Z., M.B. assisted with electrochemical tests. V.K., and A.N. conducted simulations. C.J. and B.L. assisted with XPS characterization.

Data Availability Statement

The data that support the findings of this study are available from the corresponding author upon reasonable request.

Keywords

Anion solvation, asymmetric, electrolyte design, Li metal batteries, low temperature

Received: July 3, 2023
Revised: November 7, 2023
Published online:

[1] M.-T. F. Rodrigues, G. Babu, H. Gullapalli, K. Kalaga, F. N. Sayed, K. Kato, J. Joyner, P. M. Ajayan, *Nat. Energy* **2017**, *2*, 17108.
[2] a) M. Chen, Y. Zhang, G. Xing, S.-L. Chou, Y. Tang, *Energy Environ. Sci.* **2021**, *14*, 3323; b) J. Holoubek, H. Liu, Z. Wu, Y. Yin, X. Xing, G. Cai, S. Yu, H. Zhou, T. A. Pascal, Z. Chen, P. Liu, *Nat. Energy* **2021**, *6*, 303; c) J. Holoubek, M. Yu, S. Yu, M. Li, Z. Wu, D. Xia, P. Bhaladhare, M. S. Gonzalez, T. A. Pascal, P. Liu, Z. Chen, *ACS Energy Lett.* **2020**, *5*, 1438; d) X. Ren, L. Zou, X. Cao, M. H. Engelhard, W. Liu, S. D. Burton, H. Lee, C. Niu, B. E. Matthews, Z. Zhu, C. Wang, B. W. Arey, J. Xiao, J. Liu, J.-G. Zhang, W.u Xu, *Joule* **2019**, *3*, 1662.
[3] J. Xu, *Nano-Micro Lett.* **2022**, *14*, 166.
[4] a) C. B. Jin, N. Yao, Y. Xiao, J. Xie, Z. Li, X. Chen, B. Q. Li, X. Q. Zhang, J. Q. Huang, Q. Zhang, *Adv. Mater.* **2022**, 2208340; b) J. Holoubek, K. Kim, Y. Yin, Z. Wu, H. Liu, M. Li, A. Chen, H. Gao, G. Cai, T. A. Pascal, P. Liu, Z. Chen, *Energy Environ. Sci.* **2022**, *15*, 1647.
[5] a) H. Cheng, Q. Sun, L. Li, Y. Zou, Y. Wang, T. Cai, F. Zhao, G. Liu, Z. Ma, W. Wahyudi, Q. Li, J. Ming, *ACS Energy Lett.* **2022**, *7*, 490; b) K. Xu, Y. Lam, S. S. Zhang, T. R. Jow, T. B. Curtis, *J. Phys. Chem. C* **2007**, *111*, 7411; c) M. Winter, B. Barnett, K. Xu, *Chem. Rev.* **2018**, *118*, 11433.
[6] a) J. Xu, X. Ji, J. Zhang, C. Yang, P. Wang, S. Liu, K. Ludwig, F.u Chen, P. Kofinas, C. Wang, *Nat. Energy* **2022**, *7*, 186; b) D. Chen, M. A. Mahmoud, J.-H. Wang, G. H. Waller, B. Zhao, C. Qu, M. A. El-Sayed, M. Liu, *Nano Lett.* **2019**, *19*, 2037; c) C. V. Amanchukwu, Z. Yu, X. Kong, J. Qin, Y. Cui, Z. Bao, *J. Am. Chem. Soc.* **2020**, *142*, 7393; d) Y. Watanabe, S. Kinoshita, S. Wada, K. Hoshino, H. Morimoto, S. Tobishima, *J. Power Sources* **2008**, *179*, 770; e) D. M. Seo, S. Reininger, M. Kutcher, K. Redmond, W. B. Euler, B. L. Lucht, *J. Phys. Chem. C* **2015**, *119*, 14038; f) N. Chapman, O. Borodin, T. Yoon, C. C. Nguyen, B. L. Lucht, *J. Phys. Chem. C* **2017**, *121*, 2135; g) O. Borodin, X. Ren, J. Vatamanu, A. Von Wald Cresce, J. Knap, K. Xu, *Acc. Chem. Res.* **2017**, *50*, 2886; h) O. Borodin, L. Suo, M. Gobet, X. Ren, F. Wang, A. Faraone, J. Peng, M. Olguin, M. Schroeder, M. S. Ding, E. Gobrogge, A. Von Wald Cresce, S. Munoz, J. A. Dura, S. Greenbaum, C. Wang, K. Xu, *ACS Nano* **2017**, *11*, 10462; i) K. C. Kim, T. Liu, S. W. Lee, S. S. Jang, *J. Am. Chem. Soc.* **2016**, *138*, 2374.
[7] a) Z. Jiang, J. Mo, C. Li, H.-W. Li, Q. Zhang, Z. Zeng, J. Xie, Y. Li, *Energy Environ. Mater.* **2022**, 12440; b) T. Li, X.-Q. Zhang, N. Yao, Y.-X. Yao, L.-P. Hou, X. Chen, M.-Y. Zhou, J.-Q. Huang, Q. Zhang, *Angew. Chem.* **2021**, *133*, 22865; c) J.-F. Ding, R. Xu, N. Yao, X. Chen, Y. Xiao, Y.-X. Yao, C. Yan, J. Xie, J.-Q. Huang, *Angew. Chem.* **2021**, *60*, 11442; d) W. Wahyudi, X. Guo, V. Ladelta, L. Tsetseris, M. I. Nugraha, Y. Lin, V. Tung, N. Hadjichristidis, Q. Li, K. Xu, J. Ming, T. D. Anthopoulos, *Adv. Sci.* **2022**, *9*, 2202405.
[8] D. Penley, S. P. Vicchio, R. B. Getman, B. Gurkan, *Front. Energy Res.* **2021**, 570.
[9] G. G. Eshetu, X. Judez, C. Li, M. Martinez-Ibañez, I. Gracia, O. Bondarchuk, J. Carrasco, L. M. Rodriguez-Martinez, H. Zhang, M. Armand, *J. Am. Chem. Soc.* **2018**, *140*, 9921.
[10] J.-C. Lassègues, J. Grondin, C. Aupetit, P. Johansson, *J. Phys. Chem. A* **2009**, *113*, 305.
[11] a) Z. Zhu, Y. Zhou, P. Yan, R. S. Vemuri, W.u Xu, R. Zhao, X. Wang, S. Thevuthasan, D. R. Baer, C.-M. Wang, *Nano Lett.* **2015**, *15*, 6170;

b) Y. Zhang, M. Su, X. Yu, Y. Zhou, J. Wang, R. Cao, W.u Xu, C. Wang, D. R. Baer, O. Borodin, K. Xu, Y. Wang, X.-L. Wang, Z. Xu, F. Wang, Z. Zhu, *Anal. Chem.* **2018**, *90*, 3341.
[12] D. M. Chipman, *J. Chem. Phys.* **2003**, *118*, 9937.
[13] B. D. Adams, J. Zheng, X. Ren, W. Xu, J.-G. Zhang, *Adv. Energy Mater.* **2018**, *8*, 1702097.
[14] D. Aurbach, M. L. Daroux, P. W. Faguy, E. Yeager, *J. Electrochem. Soc.* **1988**, *135*, 1863.
[15] a) G. G. Eshetu, T. Diemant, S. Grugeon, R. J. Behm, S. Laruelle, M. Armand, S. Passerini, *ACS Appl. Mater. Interfaces* **2016**, *8*, 16087; b) H. Sun, G. Zhu, Y. Zhu, M.-C. Lin, H. Chen, Y.-Y. Li, W. H. Hung, B. Zhou, X. Wang, Y. Bai, M. Gu, C.-L. Huang, H.-C. Tai, X. Xu, M. Angell, J.-J. Shyue, H. Dai, *Adv. Mater.* **2020**, *32*, 2001741.
[16] a) P. Ma, P. Mirmira, C. V. Amanchukwu, *ACS Cent. Sci.* **2021**, *7*, 1232; b) J. Holoubek, Q. Yan, H. Liu, E. J. Hopkins, Z. Wu, S. Yu, J. Luo, T. A. Pascal, Z. Chen, P. Liu, *ACS Energy Lett.* **2022**, *7*, 675.